Linear resistivity and Sachdev-Ye-Kitaev (SYK) spin liquid behavior in a quantum critical metal with spin-1/2 fermions

Peter Cha[a,1], Nils Wentzell[b], Olivier Parcollet[b,c], Antoine Georges[b,d,e,f], and Eun-Ah Kim[a]

[a]Department of Physics, Cornell University, Ithaca, NY 14853; [b]Center for Computational Quantum Physics, The Flatiron Institute, New York, NY, 10010; [c]Université Paris-Saclay, CNRS, CEA, Institut de physique théorique, 91191, Gif-sur-Yvette, France; [d]Collège de France, 75005 Paris, France; [e]Centre de Physique Théorique, Ecole Polytechnique, CNRS, 91128 Palaiseau Cedex, France; and [f]Department of Quantum Matter Physics, University of Geneva, 1211 Geneva 4, Switzerland

Edited by Subir Sachdev, Harvard University, Cambridge, MA, and approved June 22, 2020 (received for review February 20, 2020)

"Strange metals" with resistivity depending linearly on temperature *T* down to low *T* have been a long-standing puzzle in condensed matter physics. Here, we consider a lattice model of itinerant spin-1/2 fermions interacting via onsite Hubbard interaction and random infinite-ranged spin–spin interaction. We show that the quantum critical point associated with the melting of the spin-glass phase by charge fluctuations displays non-Fermi liquid behavior, with local spin dynamics identical to that of the Sachdev-Ye-Kitaev family of models. This extends the quantum spin liquid dynamics previously established in the large-*M* limit of *SU*(*M*) symmetric models to models with physical *SU*(2) spin-1/2 electrons. Remarkably, the quantum critical regime also features a Planckian linear-*T* resistivity associated with a *T*-linear scattering rate and a frequency dependence of the electronic self-energy consistent with the marginal Fermi liquid phenomenology.

Planckian metals | strange metals | marginal Fermi liquid | Sachdev-Ye-Kitaev models | cuprate superconductors

T-linear resistivity is a central enigma of correlated quantum matter. A universally observed feature of cuprate high T_c superconductors (recent reviews are in refs. 1 and 2), it has been reported in several other materials with correlated electrons and has also been the subject of recent investigations in the context of cold atomic gases in optical lattices (3, 4). For "bad metals" (5, 6) corresponding to a resistivity larger than the Mott–Ioffe–Regel (MIR) value (i.e., when the nominal mean-free path deduced from the application of a simple Drude formula is smaller than the lattice spacing), this phenomenon can be rationalized using rather general theoretical considerations at high temperatures (7–14). In contrast, a microscopic understanding remains rather elusive for metals displaying T-linear resistivity smaller than the MIR value and persisting down to low temperature. In pursuit of a theoretical understanding of this puzzle, the marginal Fermi liquid (MFL) conjecture (15, 16) was put forward early on. This approach considers fluctuations with $1/t$ scaling, where t is time, and scattering electrons with a T-linear scattering rate $\mathrm{Im}\Sigma(\omega = 0, T) \propto T$. This phenomenology lacks a microscopic fermionic model in which this is realized, however, although $1/t$ scaling was found in dissipative quantum XY models recently (17, 18). One strategy toward a microscopic theory has been to investigate the role of quantum critical fluctuations leading to non-Fermi liquid (non-FL) behavior (19, 20). However, field theoretic approaches for various itinerant fermion quantum critical points (QCPs) typically predict a different power law (21–23), and sign problem free quantum Monte Carlo found little temperature dependence in the scattering rate (24). Hence to the best of our knowledge, microscopic studies of QCP in models of itinerant spin-1/2 fermions have yet to find a T-linear scattering rate.

Another elusive state whose pursuit was motivated by cuprate phenomenology is the quantum spin liquid (QSL) (25). In efforts to establish a QSL ground state in a microscopic model, Sachdev and Ye (SY) (26) studied a spin model with quenched random interactions on a fully connected lattice. Remarkably, the model has an exactly solvable limit when one extends the spin symmetry group to $SU(M)$ and takes the $M \to \infty$ limit. An exciting finding of ref. 26 in this solvable limit was a QSL ground state with slowly decaying local spin–spin correlations in the long-time limit $\langle S(t) \cdot S(0) \rangle \sim 1/t$, where t is real time. Doping this model in the spirit of a t-J model, ref. 27 found, again at $M = \infty$, a QCP separating the SY phase from a FL ground state. The quantum critical regime was found to retain the QSL correlations of the SY model and remarkably, to display bad metal behavior with T-linear resistivity despite a single-particle scattering rate behaving as $\sqrt{T}$ (27). However, a numerical study of the SY model with physical $SU(2)$ spins found a spin glass (SG) ordered ground state instead of the QSL ground state seen in the large-M limit (28). The relevance of SY behavior to physical spin-1/2 electrons and to the T-linear resistivity problem in real materials is therefore a major open question.

In this article, we provide a major step toward answering this question in the positive by 1) considering a lattice model in

Significance

In "Planckian metals," electrons dissipate energy at the fastest possible rate allowed by the fundamental laws of quantum mechanics, resulting in a linear temperature dependence of their electrical resistivity. Although observed for a number of quantum materials, this phenomenon lacks a general theoretical understanding and is often considered as one of the prominent fundamental questions in condensed matter physics. Here, we show that Planckian dissipation and a behavior consistent with the "marginal Fermi liquid" phenomenology emerge in the quantum critical regime separating a Mott insulating spin glass and a Fermi liquid. By establishing this behavior in an explicit model solvable by state-of-the-art computational methods, our theory paves the way toward a deeper understanding of Planckian or "strange" metals.

Author contributions: O.P., A.G., and E.-A.K. designed research; P.C., N.W., O.P., A.G., and E.-A.K. performed research; N.W. and O.P. contributed new reagents/analytic tools; P.C., N.W., O.P., A.G., and E.-A.K. analyzed data; and P.C., N.W., O.P., A.G., and E.-A.K. wrote the paper.

The authors declare no competing interest.

This article is a PNAS Direct Submission.

Data deposition: The data analyzed in this article are available at the Figshare repository (https://doi.org/10.6084/m9.figshare.12627419).

[1]To whom correspondence may be addressed. Email: pjc277@cornell.edu.

This article contains supporting information online at https://www.pnas.org/lookup/suppl/doi:10.1073/pnas.2003179117/-/DCSupplemental.

First published July 22, 2020.

which the SG phase can be quantum melted at the QCP and 2) providing an explicit numerical solution of this model directly for spin-1/2 $SU(2)$ fermions. We find, remarkably, that the quantum critical regime displays SY spin-liquid correlations and a scattering rate linear in temperature, leading to T-linear resistivity down to $T=0$ at the QCP. Our numerical results are consistent with the MFL phenomenology.

We consider a "t-U-J model" of itinerant spin-1/2 $SU(2)$ fermions with an onsite repulsive-U Hubbard interaction and a random infinite-ranged spin–spin coupling, at half-filling. Using the extended dynamical mean-field theory framework (EDMFT) (29–32) and numerical methods detailed below, we obtain the phase diagram displayed in Fig. 1. At $t/U\to 0$, we have a Mott insulating SG phase (Fig. 1), where the fermions are localized onsite and the model reduces to the disordered Heisenberg model. SG order is found below a freezing temperature $T_g\approx 0.14J$ for $t/U=0$ as previously established (28, 33) (*SI Appendix*, sections A and B). As t/U is increased, the single-occupancy constraint is relaxed, and the charge fluctuations lead to quantum melting of SG order at a QCP $(t/U)_c\approx 0.31$ separating the SG from an FL phase at low-enough temperature for $(t/U)>(t/U)_c$ (blue points in Fig. 1). Our key finding is a quantum critical region emanating from the QCP with QSL spin dynamics identical to that of the SY model (26) and T-linear MFL scattering rate $\mathrm{Im}\Sigma(\omega\to 0,T)\propto T$ (red points in Fig. 1), leading to T-linear resistivity as shown below.

More precisely, our model Hamiltonian reads

$$H=-\sum_{\langle ij\rangle,s=\uparrow,\downarrow} t_{ij}\, c_{is}^{\dagger}c_{js}+U\sum_i n_{i\uparrow}n_{i\downarrow}-\sum_{i<j}\frac{J_{ij}}{\sqrt{\mathcal{N}}}\vec{S}_i\cdot\vec{S}_j. \quad [1]$$

In this expression, J_{ij} are quenched random Heisenberg interactions (33) drawn from a Gaussian distribution with $\langle J_{ij}\rangle=0$ and $\langle J_{ij}^2\rangle=J^2$, $\mathcal{N}$ is the number of sites, and $\vec{S}_i=\frac{1}{2}c_{is}^{\dagger}\vec{\sigma}_{ss'}c_{is'}$, with $\vec{\sigma}$ the Pauli matrices. The model can be formulated either on the infinite connectivity $z\to\infty$ Bethe lattice with $t_{ij}=t/\sqrt{z}$ or on a fully connected lattice with Gaussian distributed random t_{ij} with $\langle t_{ij}\rangle=0$ and $\langle t_{ij}^2\rangle=t^2/\mathcal{N}$, leading to identical equations in the phase without magnetic ordering after replica averaging (34). We restrict ourselves to the half-filling case $\mu=U/2$ and choose $J=0.5t$. A study of the $SU(M)$ version of this model in the large-M limit at half-filling is in ref. 35.

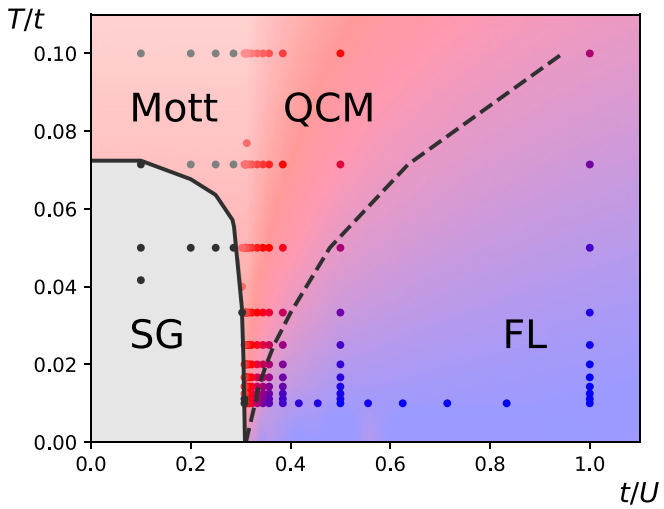

Fig. 1. Calculated phase diagram of the *t-U-J* model [1] at $J/t=0.5$. Solid black curve indicates a second-order phase transition to SG order. Round markers represent parameters for which we have explicitly solved the model. Markers have been colored red where we find a quantum critical metal (QCM) with QSL spin dynamics and blue where we find an FL. Background shading interpolates between the explicitly solved points. Dashed black curve indicates the cross-over between QCM and FL regimes. Gray markers indicate Mott insulating solutions. Black markers indicate SG ordered solutions.

To investigate the phase diagram of model [1], both the onsite repulsion in the charge channel and the random interaction in the spin channel need to be tamed. This is achieved using the EDMFT framework and the replica trick. In this framework, the calculation of the local Green's function and spin–spin correlation function is mapped onto the solution of a local "quantum impurity" problem subject to a self-consistency condition (26, 27, 29, 33, 34, 36–38). This mapping is exact in the infinite connectivity $z\to\infty$ or infinite volume limit $\mathcal{N}\to\infty$ of the two formulations of the model discussed above.

The resulting local effective action, after disorder averaging and making a replica diagonal ansatz, reads

$$S_{\text{eff}}=-\beta\sum_{n,s}c_s^{\dagger}\left(i\omega_n+\mu-\Delta(i\omega_n)\right)c_s+U\int_0^{\beta}d\tau\, n_{\uparrow}n_{\downarrow}$$
$$-\frac{J^2}{2}\int_0^{\beta}d\tau\, d\tau'\; Q(\tau-\tau')\vec{S}(\tau)\cdot\vec{S}(\tau'). \quad [2]$$

In this expression, $\beta=1/T$ ($k_B=1$) is the inverse temperature, $\tau\in[0,\beta]$ stands for imaginary time, and $\omega_n=(2n+1)\pi/\beta$ are Matsubara frequencies. The dynamical mean-field (hybridization function) Δ and effective spin–spin retarded interaction Q are subject to the following self-consistency conditions:

$$\Delta(\tau)=t^2G(\tau),\quad Q(\tau-\tau')=\frac{1}{3}\left\langle\vec{S}(\tau)\cdot\vec{S}(\tau')\right\rangle, \quad [3]$$

in which the local Green's function $G(\tau)\equiv-\langle Tc_s(\tau)c_s^{\dagger}(0)\rangle$ and the local spin–spin correlator $\left\langle\vec{S}(\tau)\cdot\vec{S}(\tau')\right\rangle$ are to be computed with the local effective action [2]. Noting that $i\omega_n+\mu-\Delta(i\omega_n)$ is the inverse effective one-body propagator of this action, a fermionic self-energy can be defined from Dyson's equation as

$$\Sigma(i\omega_n)=i\omega_n+\mu-\Delta(i\omega_n)-G^{-1}(i\omega_n). \quad [4]$$

The local action [2] still presents a strongly correlated problem. SY (26) made further progress on the random Heisenberg model by extending the spin symmetry to $SU(M)$ and taking the $M\to\infty$ limit, which allows for an analytical calculation of the spin–spin correlator of [2] and reduces the self-consistent problem to a nonlinear integral equation. This $M\to\infty$ limit was extended to itinerant fermions within the t-J_{ij} model by Parcollet and Georges (PG) (27), who obtained an FL regime of the doped model at low T, and a quantum critical regime associated with the proximity of the spin-liquid Mott insulator characterized by a $\sqrt{\omega},\sqrt{T}$ self-energy but remarkably, bad metal behavior with linear resistivity. Recently, fermionic versions of the random coupling problem, the so-called Sachdev-Ye-Kitaev (SYK) models (39, 40), garnered much interest with again a solvable limit for a large number of flavors $M\to\infty$. Recent works (41–45) extended the mechanism of PG (27) for linear-T resistivity to a lattice of SYK "quantum dots" with hopping. Interestingly, when SYK dots are coupled to another band of otherwise free and translationally invariant (uniform hopping) fermions, not only does the T-linear resistivity extend down to zero temperature, but the mechanism switches to that driven by the MFL T-linear scattering rate (46, 47).

For the physical limit of a single flavor of spin-1/2 fermions that is of our interest, the self-consistency equations above require computing two- and four-point correlators in the local

model with $SU(2)$ symmetry. We use an implementation of Rubtsov's continuous-time interaction–expansion quantum Monte Carlo (CT-INT) (48) algorithm, which is based on the TRIQS library (49). The algorithm works in imaginary time, so we will discuss most of our results directly on the imaginary axis without analytic continuation, except in the discussion of transport. Our implementation determines the local spin–spin correlator from the impurity three-point vertex function rather than through an operator insertion measurement. This algorithmic improvement allows for a drastic speedup of the calculations.

Let us first consider the long-time spin dynamics. In Fig. 2, we display the local spin–spin correlation function $Q(\tau)$ at a fixed low temperature $T/t=0.01$ for various t/U approaching the QCP at $(t/U)_c\approx 0.31$ from the FL limit cutting the phase diagram Fig. 1 along the horizontal axis. In Fig. 2, *Inset*, we also display how $Q(\tau)$ varies upon raising temperatures for fixed $t/U=0.357$ making a vertical cut in the phase diagram slightly away from the QCP. Since we work in the Matsubara formalism, a zero-temperature long-time asymptotic form $Q(t)\sim 1/t^{\alpha}$ transforms into a scaling function $Q(\tau)\sim((\pi/\beta)/\sin(\pi\tau/\beta))^{\alpha}$, and the data should be examined away from $\tau=0,\beta$. Examining correlators at $\tau=\beta/2$ is an established method of analyzing long-time, low-frequency behavior (50). However, as we are interested in the scaling exponent, we examine the full τ dependence of the spin–spin correlator in a large region around $\tau=\beta/2$. Away from the critical point, for $t/U=1.0$, we obtain the FL behavior at long-time $Q(t)\sim 1/t^2$ ($\alpha=2$). The closer one gets to the critical point, the longer it takes to reach this asymptotic regime, reflecting the decrease of the FL coherence scale close to the critical point. Once in the quantum critical regime, for $t/U=(t/U)_c\approx 0.31$, the long-time spin dynamics crosses over to $Q(t)\sim 1/t$ ($\alpha=1$), which is the same power law as in the SY $M=\infty$ model. The QSL to FL cross-over is also visible in the temperature cut shown in Fig. 2, *Inset*, where we observe the cross-over from $1/t$ within the quantum critical fan above the FL coherence temperature to $1/t^2$ at low temperatures. The phase classification at each point in Fig. 1 follows the above criterion to identify the FL regime and the QSL regime.

These results establish that our $SU(2)$ t-U-J model has, in the quantum critical regime, the same QSL local spin dynamics ($\alpha=1$) as the SY model in the $M=\infty$ limit. Renormalization group (RG) methods should prove useful in establishing analytically our numerical findings for $SU(2)$. For simplified versions of the effective action [**2**] (e.g., involving only localized spins) (51), RG methods have indeed established (51–61) that the $Q(t)\sim 1/t$ spin-liquid behavior is the only one consistent with the self-consistency condition [**3**]. This was recently extended to the QCP obtained by doping the $U=\infty$ model (62).

Let us now consider the one-particle properties, encoded by the self-energy Σ. In the FL regime for $(t/U)_c\ll(t/U)$, the self-energy has the low-energy expansion*:

$$\mathrm{Im}\Sigma(i\omega_n,T)\approx\left(1-\frac{1}{Z}\right)\omega_n+\frac{\omega_n^2-(\pi T)^2}{E}+O(\omega_n^3). \qquad [5]$$

In the small hopping limit $(t/U)\ll(t/U)_c$, Σ diverges at low frequencies as $1/\omega_n$, indicating a transition into an insulating phase (*SI Appendix*, section C). We examine the cross-over from the FL to the quantum critical regime in several ways. First, a direct consequence of [**5**] is that the self-energy at the first Matsubara frequency is linear in temperature with vanishing quadratic corrections (63): $\mathrm{Im}\Sigma(i\omega_0=i\pi T)=(1-1/Z)\pi T+\mathcal{O}(T^3)$. Deviation from linearity in T at a temperature T^* signals the FL coherence scale and hence, the cross-over to the quantum critical regime. This is illustrated in Fig. 3*A*: when t/U approaches $(t/U)_c$, the self-energy increases, and T^* (indicated by arrows on the figure) decreases. More precisely, we extract the quasiparticle residue Z and the coherence scale E by fitting the functional form [**5**] to the low-energy data using weighted least squares. Fig. 3*B* shows that Z and E vanish at the QCP. The susceptibility to SG order is given by (37, 38) $\chi_{sg}\propto\chi^2/(1-J^2\chi^2)$ with χ the local susceptibility. As shown in Fig. 3, we find that $1-J\chi$ also vanishes close to the QCP, indicating the boundary of the SG phase. Within our numerical accuracy, we cannot however exclude that $1-J\chi$ vanishes at a slightly larger value of t/U than E, possibly indicating a small intervening region of metallic SG (62).

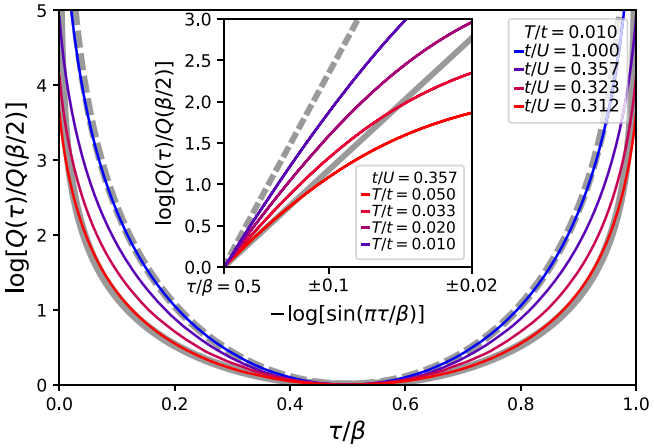

Fig. 2. Spin susceptibility $\log[Q(\tau)/Q(\beta/2)]$ vs. τ/β for $J/t=0.5$ and $T/t=0.01$, across several t/U. Gray curves show $(1/\sin\pi\tau/\beta)^{\alpha}$ with $\alpha=1$ (solid) and $\alpha=2$ (dashed). Color scheme follows the blue (FL) and red (QSL) gradient of Fig. 1. (*Inset*) Spin susceptibility $\log[Q(\tau)/Q(\beta/2)]$ vs. $-\log[\sin(\pi\tau/\beta)]$, for $J/t=0.5$ and $t/U=0.357$, across a range of T, demonstrating scaling behavior of $Q(\tau)$ near $\tau=\beta/2$. Gray curves show $\alpha=1,2$ (solid and dashed, respectively).

In order to analyze the QCP, we attempt to scale the self-energy for t/U close to $(t/U)_c$, for our lowest temperature $T/t=0.01$, with an ansatz of the form

$$\mathrm{Im}\Sigma(i\omega_n)\approx\mathrm{Im}\Sigma(0)+f\left(\frac{\omega_n}{\omega^*}\right), \qquad [6]$$

which applies for ω_n and ω^* smaller than the high-energy cutoff J but ω_n/ω^* otherwise arbitrary. We determine numerically $\mathrm{Im}\Sigma(0)$, ω^*, and the scaling function f by requesting that optimal data collapse is obtained, using a minimization procedure. We obtain a remarkable collapse of the data, presented in Fig. 4*A*, with ω^* presented in Fig. 3*B*.

For $\omega<\omega^*$, the ansatz [**6**] has to reproduce [**5**], which implies $Z\propto\omega^*$ (for $\omega^*\to 0$), and $E\propto(\omega^*)^2$; hence, $E\propto Z^2$, as illustrated in Fig. 3*B*, *Inset*. Note however that the ω^* obtained from the data collapse does not perfectly vanish close to the QCP, which may be due to numerical uncertainty, or possibly to a weakly first-order transition or to an intervening metallic SG phase as mentioned above. In the quantum critical regime (i.e., for $\omega>\omega^*$), the self-energy is very well described by an MFL form $\mathrm{Im}\Sigma(\omega_n)\propto\Sigma(0)+a\omega_n\ln\omega_n/b$ (Fig. 4*A*, *Inset*). However, the low-temperature behavior obtained in the large-M limit (26) (i.e., $\sqrt{\omega_n}$) cannot be excluded given our data. Indeed, the CT-INT algorithm is faced with a sign problem at low T, which prevents us from reaching the very low-temperature regime

*In a FL, the real-frequency dependence of the self-energy is well known to be $-\mathrm{Im}\Sigma(\omega)\sim(\omega^2+(\pi T)^2)/E$. When the self-energy is analytically continued to Matsubara frequencies, the imaginary part of self-energy gains a linear term in frequency from the low-frequency expansion of $\mathrm{Re}\Sigma(\omega)$, so that $-\mathrm{Im}\Sigma(i\omega_n)\sim\omega_n$.

PHYSICS

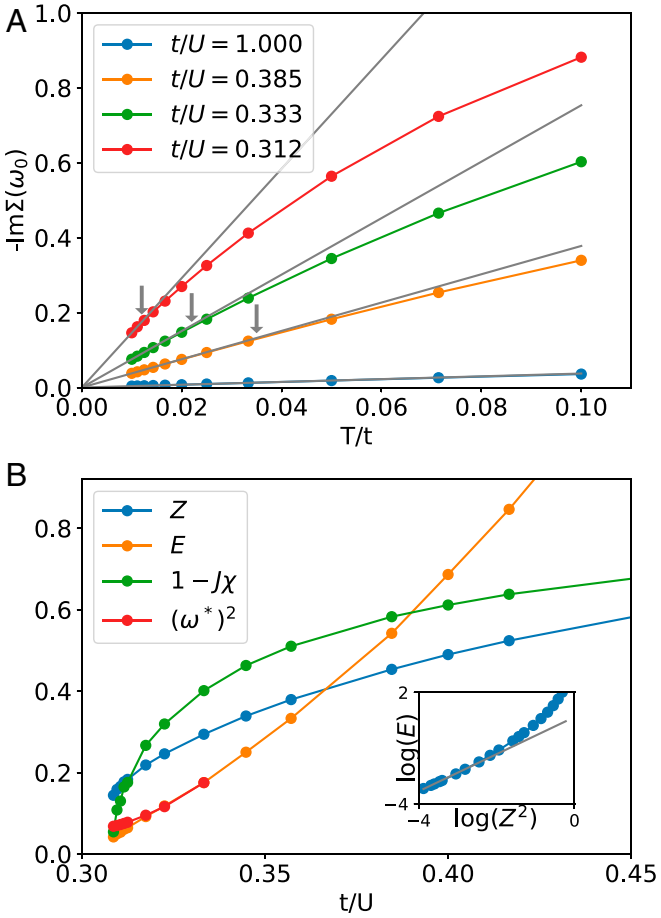

Fig. 3. (*A*) Imaginary part of the self-energy at the first Matsubara point $-\mathrm{Im}\Sigma(i\omega_0 = i\pi T)$ vs. temperature T, for a range of t/U. Solid gray lines stand for the FL prediction of $\mathrm{Im}\Sigma(i\omega_0) \propto T$ from the lowest temperature. Arrows indicate the FL coherence temperature T^* for each value of t/U. The solution at $t/U = 1.0$ remains in the FL regime over the entire range of temperature considered. (*B*) Quasiparticle residue Z and coherence scale E as obtained by fitting [5] to the self-energy data, ordering criterion for the SG phase $1 - J\chi$, and the energy scale determined from scaling plot $(\omega^*)^2$ vs. t/U. (*Inset*) $\log E$ vs. $\log Z^2$ illustrating a dependency $E \propto Z^2$ close to the QCP. Gray line with slope 1 is plotted to guide the eye.

required to settle this question. This conclusion holds both for the scaling function f and for a direct analysis of the self-energy at $t/U = (t/U)_c$.

The value of the self-energy at zero-frequency $\mathrm{Im}\Sigma(0)$ is of crucial importance for transport properties. In Fig. 4*C*, we show $\mathrm{Im}\Sigma(0)$ extracted from the scaling analysis, for various U close to the QCP. We find that $\mathrm{Im}\Sigma(0) \propto T$ at low temperature at the QCP. This is confirmed in Fig. 4*D*: $\mathrm{Im}\Sigma(i\omega)$ obtained (by interpolation) for fixed imaginary frequency $i\omega$ is linear with temperature, with a slope weakly dependent on the frequency.

Let us finally turn to the direct current (DC) resistivity in the quantum critical region. The Kubo formula reduces to the polarization bubble (vertex corrections vanish in this quantity in Dynamical Mean Field Theory [DMFT]):

$$\sigma_{\mathrm{DC}} = \frac{2\pi e^2}{\hbar} \int d\omega \frac{\beta}{4\cosh^2(\beta\omega/2)} \int d\epsilon\, \phi(\epsilon) A(\epsilon,\omega)^2. \qquad [7]$$

This expression only relies on vanishing vertex corrections, which is valid in DMFT as well as in other contexts, such as large-N SYK models.[†] In this expression, ϵ is the energy of a bare single-particle state within the band, $A(\epsilon,\omega) = -(1/\pi)\mathrm{Im}\,G^R(\epsilon,\omega)$ is the energy-(momentum-)resolved spectral function, and $\phi(\epsilon)$ is the transport function $\phi(\epsilon) = \sum_{\mathbf{k}} (\partial\epsilon_{\mathbf{k}}/\partial k_x)^2 \delta(\epsilon - \epsilon_{\mathbf{k}})$, which we take to be the sum-rule preserving expression on the Bethe lattice (e.g., ref. 10): $\phi(\epsilon) = \phi(0)[1 - (\epsilon/2t)^2]^{3/2}$. To obtain σ_{DC}, we perform an analytic continuation of the Monte Carlo data using Padé approximants (64) to obtain the real-frequency self-energy $\Sigma(\omega) = \Sigma'(\omega) + i\Sigma''(\omega)$ and the spectral function: $\pi A(\epsilon,\omega) = -\Sigma''(\omega)/[(\omega + \mu - \epsilon - \Sigma'(\omega))^2 + \Sigma''(\omega)^2]$. The resulting resistivity $\rho_{\mathrm{DC}} = 1/\sigma_{\mathrm{DC}}$ vs. temperature T is plotted in Fig. 4*C*, clearly consistent with T-linear resistivity within numerical accuracy.

The origin of this behavior can be directly related to the T-linear behavior of the scattering rate $\Sigma''(0)$. Indeed, observing that the latter is a much smaller scale than the bandwidth at low T, the integral over ϵ can be approximated as

$$\int d\epsilon\, \phi(\epsilon) A(\epsilon,\omega)^2 \sim \frac{\phi[\omega + \mu - \Sigma'(\omega)]}{2\pi|\Sigma''(\omega)|}. \qquad [8]$$

Due to the Fermi factor only, $|\omega| \lesssim T$ is relevant for the frequency integral, so that the right-hand side of this expression can be replaced by its Fermi surface contribution $\omega = 0$ (*SI Appendix*, section D). Observing that $\mu - \Sigma'(0) = 0$, we finally obtain

$$\sigma_{\mathrm{DC}} = \frac{e^2\phi(0)}{\hbar} \int \frac{\beta d\omega}{4\cosh^2(\beta\omega/2)} \frac{1}{|\Sigma''(\omega)|} \sim \frac{e^2\phi(0)}{\hbar T}. \qquad [9]$$

$\rho_0 = (\hbar/e^2)/(\phi(0)/t)$ can be taken as the order of magnitude of the MIR resistivity (10), so that we obtain at the QCP $\rho_{\mathrm{DC}}/\rho_0 \sim T/t$ down to the lowest value of T we could reach.

We would like to emphasize that both the mechanism and the physical meaning of this T-linear resistivity are different from the ones reported in ref. 27 and in the SYK $M \to \infty$ lattice models (41–45). There, the scattering rate had a $\sim\sqrt{T}$ temperature dependence and dominated the band dispersion in the incoherent metal regime $T > T^*$, resulting in the resistivity being proportional by the square of the scattering rate and larger than the MIR value. Here, in contrast, the scattering rate is T linear (Planckian) and small at low T, and the band dispersion dominates, resulting in linear resistivity down to low T. The present mechanism is also distinct from the generic bad metal behavior of lattice models at very high T comparable with the bandwidth (7, 8, 10, 11, 14): there, the scattering is constant, and the T-linear behavior is associated with the T dependence of thermodynamic quantities such as the kinetic energy $\sim 1/T$, which play the role of an effective carrier number. We have checked (*SI Appendix*, section E) that in contrast the kinetic energy of our model is constant in the range of T of interest.

In this work, we considered the insulator to metal transition and quantum melting by charge fluctuations of the SG ground state of the $SU(2)$ random-bond Heisenberg model. At the QCP separating the SG from the FL, we find a non-FL state with long-lived spin correlations $\langle \vec{S}(t) \cdot \vec{S}(0) \rangle \sim 1/t$ [as in the large-M limit of the $SU(M)$ SY model] and a T-linear resistivity arising from a T-linear (Planckian) scattering rate $\mathrm{Im}\Sigma(\omega = 0, T) \propto T$. In the temperature range accessible in this work, this quantum critical regime is compatible with a marginal Fermi phenomenology $\Sigma(\omega) \sim -\omega \log \omega$. The Planckian scattering rate and MFL behavior are driven by local quantum critical fluctuations from the

[†]In a theory in which momentum dependence (in contrast to frequency dependence) can be neglected in both the self-energy and the vertex, the vertex corrections to the conductivity vanish because the current is odd in momentum.

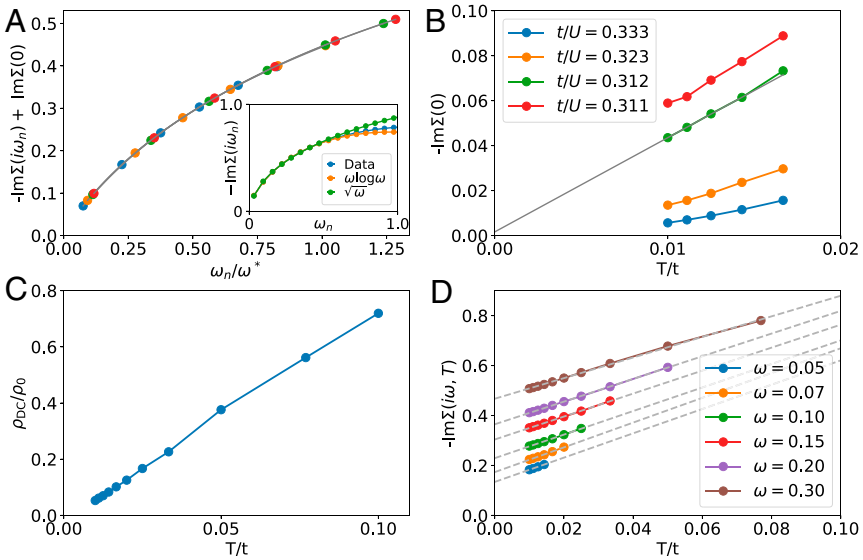

Fig. 4. (*A*) Imaginary part of self-energy with the scattering rate subtracted $-(\mathrm{Im}\Sigma(i\omega_n) - \mathrm{Im}\Sigma(0))$ vs. the scaled frequency ω/ω^* for various values of t/U near the QCP at $T/t = 0.01$, demonstrating the collapse onto the universal scaling function $f(\omega/\omega^*)$ (gray solid curve). Color scheme follows *B*. (*Inset*) Imaginary part of self-energy $-\mathrm{Im}\Sigma(i\omega_n)$ vs. Matsubara frequencies ω_n at the QCP $t/U = 0.312$ and lowest accessible temperature $T/t = 0.01$. Also shown are low-frequency fits of self-energy to the MFL form $c + a\omega_n \log \omega_n/b$ (orange) and the SYK form $c + a\sqrt{\omega_n} + b\omega_n$ (green). (*B*) Scattering rate $-\mathrm{Im}\Sigma(0)$ vs. temperature T/t at various values of t/U near the QCP. At the QCP ($t/U = 0.312$, green), the scattering rate is T linear (linear fit in gray), in contrast to the quadratic behavior in the FL regime (blue). (*C*) Resistivity ρ_{DC}/ρ_0 vs. temperature T/t at the QCP computed with the analytically continued Green's function. The unit of resistivity is the MIR value $\rho_0 = \hbar/e^2\phi(0)$, where ϕ is the transport function. (*D*) Imaginary part of self-energy at fixed, interpolated values of Matsubara frequency $-\mathrm{Im}\Sigma(i\omega = \text{fixed}, T)$ vs. temperature T/t at the QCP $t/U = 0.312$, for various fixed values of frequency.

QCP. Fully establishing this behavior down to zero temperature may require a new generation of quantum impurity solvers, such as real-time diagrammatic Monte Carlo (65, 66). Another open question is whether our results for the scattering rate also apply to the doped case recently considered in ref. 62. Also, finding the RG fixed point associated with our metal insulator transition QCP remains an open question.

Data Availability. The data analyzed in this article are available at the Figshare repository (67).

ACKNOWLEDGMENTS. We thank Chao-Ming Jian, Aavishkar Patel, Subir Sachdev, and Anirvan Sengupta for useful discussions. P.C. and E.-A.K. are supported by US Department of Energy, Office of Basic Energy Sciences, Division of Materials Science and Engineering Award DE-SC0018946. The Flatiron Institute is a division of the Simons Foundation.

1. C. Proust, L. Taillefer, The remarkable underlying ground states of cuprate superconductors. *Annu. Rev. Condens. Matter Phys.* **10**, 409–429 (2019).
2. C. M. Varma, Linear in temperature resistivity and associated mysteries. arXiv: 1908.05686 (15 August 2019).
3. P. T. Brown *et al.*, Bad metallic transport in a cold atom Fermi-Hubbard system. *Science* **363**, 379–382 (2019).
4. W. Xu, W. McGehee, W. Morong, B. DeMarco, Bad-metal relaxation dynamics in a Fermi lattice gas. *Nat. Commun.* **10**, 1588 (2019).
5. V. J. Emery, S. A. Kivelson, Superconductivity in bad metals. *Phys. Rev. Lett.* **74**, 3253–3256 (1995).
6. N. Hussey, K. Takenaka, H. Takagi, Universality of the Mott-Ioffe-Regel limit in metals. *Phil. Mag.* **84**, 2847–2864 (2004).
7. O. Gunnarsson, M. Calandra, J. E. Han, Colloquium: Saturation of electrical resistivity. *Rev. Mod. Phys.* **75**, 1085–1099 (2003).
8. G. Pálsson, G. Kotliar, Thermoelectric response near the density driven Mott transition. *Phys. Rev. Lett.* **80**, 4775–4778 (1998).
9. G. Palsson, "Computational studies of thermoelectricity in strongly correlated systems," PhD thesis, Rutgers University, New Brunswick, NJ (2001).
10. X. Deng *et al.*, How bad metals turn good: Spectroscopic signatures of resilient quasiparticles. *Phys. Rev. Lett.* **110**, 086401 (2013).
11. E. Perepelitsky *et al.*, Transport and optical conductivity in the Hubbard model: A high-temperature expansion perspective. *Phys. Rev. B* **94**, 235115 (2016).
12. S. A. Hartnoll, Theory of universal incoherent metallic transport. *Nat. Phys.* **11**, 54–61 (2015).
13. C. H. Mousatov, I. Esterlis, S. A. Hartnoll, Bad metallic transport in a modified Hubbard model. *Phys. Rev. Lett.* **122**, 186601 (2019).
14. P. Cha, A. A. Patel, E. Gull, E. A. Kim, *T*-linear resistivity in models with local self-energy. arXiv:1910.07530 (16 October 2019).
15. C. M. Varma, P. B. Littlewood, S. Schmitt-Rink, E. Abrahams, A. E. Ruckenstein, Phenomenology of the normal state of Cu-O high-temperature superconductors. *Phys. Rev. Lett.* **63**, 1996–1999 (1989).
16. P. B. Littlewood, C. M. Varma, Phenomenology of the normal and superconducting states of a marginal Fermi liquid (invited). *J. Appl. Phys.* **69**, 4979–4984 (1991).
17. L. Zhu, Y. Chen, C. M. Varma, Local quantum criticality in the two-dimensional dissipative quantum XY model. *Phys. Rev. B* **91**, 205129 (2015).
18. C. M. Varma, Quantum-critical fluctuations in 2D metals: Strange metals and superconductivity in antiferromagnets and in cuprates. *Rep. Prog. Phys.* **79**, 082501 (2016).
19. D. Marel *et al.*, Quantum critical behaviour in a high-T-c superconductor. *Nature* **425**, 271–274 (2003).
20. P. Gegenwart, Q. Si, F. Steglich, Quantum criticality in heavy-fermion metals. *Nat. Phys.* **4**, 186–197 (2008).
21. J. A. Hertz, Quantum critical phenomena. *Phys. Rev. B* **14**, 1165–1184 (1976).
22. T. Moriya, *Spin Fluctuations in Itinerant Electron Magnetism* (Springer Series in Solid-State Sciences, Springer, Berlin, Germany, 1985), vol. 56.
23. A. J. Millis, Effect of a nonzero temperature on quantum critical points in itinerant fermion systems. *Phys. Rev. B* **48**, 7183–7196 (1993).
24. S. Lederer, Y. Schattner, E. Berg, S. A. Kivelson, Superconductivity and non-Fermi liquid behavior near a nematic quantum critical point. *Proc. Natl. Acad. Sci. U.S.A.* **114**, 4905–4910 (2017).
25. P. Anderson, Resonating valence bonds: A new kind of insulator?*Mater. Res. Bull.* **8**, 153–160 (1973).
26. S. Sachdev, J. Ye, Gapless spin-fluid ground state in a random quantum Heisenberg magnet. *Phys. Rev. Lett.* **70**, 3339–3342 (1993).
27. O. Parcollet, A. Georges, Non-Fermi-liquid regime of a doped Mott insulator. *Phys. Rev. B* **59**, 5341–5360 (1999).
28. D. R. Grempel, M. J. Rozenberg, Fluctuations in a quantum random Heisenberg paramagnet. *Phys. Rev. Lett.* **80**, 389–392 (1998).
29. A. M. Sengupta, A. Georges, Non-Fermi-liquid behavior near a $T = 0$ spin-glass transition. *Phys. Rev. B* **52**, 10295–10302 (1995).
30. J. L. Smith, Q. Si, Spatial correlations in dynamical mean-field theory. *Phys. Rev. B* **61**, 5184–5193 (2000).
31. R. Chitra, G. Kotliar, Effect of long range Coulomb interactions on the Mott transition. *Phys. Rev. Lett.* **84**, 3678–3681 (2000).
32. G. Kotliar *et al.*, Electronic structure calculations with dynamical mean-field theory. *Rev. Mod. Phys.* **78**, 865–951 (2006).

33. A. J. Bray, M. A. Moore, Replica theory of quantum spin glasses. *J. Phys. C Solid State Phys.* **13**, L655–L660 (1980).
34. A. Georges, G. Kotliar, W. Krauth, M. J. Rozenberg, Dynamical mean-field theory of strongly correlated fermion systems and the limit of infinite dimensions. *Rev. Mod. Phys.* **68**, 13–125 (1996).
35. S. Florens, P. Mohan, C. Janani, T. Gupta, R. Narayanan, Magnetic fluctuations near the Mott transition towards a spin liquid state. *Europhys. Lett.* **103**, 17002 (2013).
36. A. Georges, G. Kotliar, Hubbard model in infinite dimensions. *Phys. Rev. B* **45**, 6479–6483 (1992).
37. A. Georges, O. Parcollet, S. Sachdev, Mean field theory of a quantum Heisenberg spin glass. *Phys. Rev. Lett.* **85**, 840–843 (2000).
38. A. Georges, O. Parcollet, S. Sachdev, Quantum fluctuations of a nearly critical Heisenberg spin glass. *Phys. Rev. B* **63**, 134406 (2001).
39. A. Kitaev, "Hidden correlations in the Hawking radiation and thermal noise" (video recording, 2015). http://online.itp.ucsb.edu/online/joint98/kitaev/. Accessed 17 July 2020.
40. S. Sachdev, Bekenstein-Hawking entropy and strange metals. *Phys. Rev. X* **5**, 041025 (2015).
41. X. Y. Song, C. M. Jian, L. Balents, Strongly correlated metal built from Sachdev-Ye-Kitaev models. *Phys. Rev. Lett.* **119**, 216601 (2017).
42. A. A. Patel, M. J. Lawler, E. A. Kim, Coherent superconductivity with a large gap ratio from incoherent metals. *Phys. Rev. Lett.* **121**, 187001 (2018).
43. P. Zhang, Dispersive Sachdev-Ye-Kitaev model: Band structure and quantum chaos. *Phys. Rev. B* **96**, 205138 (2017).
44. A. Haldar, S. Banerjee, V. B. Shenoy, Higher-dimensional Sachdev-Ye-Kitaev non-Fermi liquids at Lifshitz transitions. *Phys. Rev. B* **97**, 241106 (2018).
45. D. Ben-Zion, J. McGreevy, Strange metal from local quantum chaos. *Phys. Rev. B* **97**, 155117 (2018).
46. D. Chowdhury, Y. Werman, E. Berg, T. Senthil, Translationally invariant non-Fermi-liquid metals with critical Fermi surfaces: Solvable models. *Phys. Rev. X* **8**, 031024 (2018).
47. A. A. Patel, J. McGreevy, D. P. Arovas, S. Sachdev, Magnetotransport in a model of a disordered strange metal. *Phys. Rev. X* **8**, 021049 (2018).
48. A. N. Rubtsov, V. V. Savkin, A. I. Lichtenstein, Continuous-time quantum Monte Carlo method for fermions. *Phys. Rev. B* **72**, 035122 (2005).
49. O. Parcollet, *et al.*, TRIQS: A toolbox for research on interacting quantum systems. *Comput. Phys. Commun.* **196**, 398–415 (2015).
50. M. Randeria, N. Trivedi, A. Moreo, R. T. Scalettar, Pairing and spin gap in the normal state of short coherence length superconductors. *Phys. Rev. Lett.* **69**, 2001–2004 (1992).
51. A. M. Sengupta, Spin in a fluctuating field: The Bose(+Fermi) Kondo models. *Phys. Rev. B* **61**, 4041–4043 (2000).
52. M. Vojta, C. Buragohain, S. Sachdev, Quantum impurity dynamics in two-dimensional antiferromagnets and superconductors. *Phys. Rev. B* **61**, 15152–15184 (2000).
53. S. Sachdev, C. Buragohain, M. Vojta, Quantum impurity in a nearly critical two dimensional antiferromagnet. *Science* **286**, 2479–2482 (1999).
54. M. Kirćan, M. Vojta, Critical properties of the Fermi-Bose Kondo and pseudogap Kondo models: Renormalized perturbation theory. *Phys. Rev. B* **69**, 174421 (2004).
55. L. Fritz, M. Vojta, Phase transitions in the pseudogap Anderson and Kondo models: Critical dimensions, renormalization group, and local-moment criticality. *Phys. Rev. B* **70**, 214427 (2004).
56. L. Fritz, S. Florens, M. Vojta, Universal crossovers and critical dynamics of quantum phase transitions: A renormalization group study of the pseudogap Kondo problem. *Phys. Rev. B* **74**, 144410 (2006).
57. L. Fritz, "Quantum phase transitions in models of magnetic impurities," PhD thesis, University of Karlsruhe, Karlsruhe, Baden-Württemberg, Germany (2006).
58. S. Sachdev, Static hole in a critical antiferromagnet: Field-theoretic renormalization group. *Phys. C Supercond.* **357**, 78–81 (2001).
59. M. Vojta, L. Fritz, Upper critical dimension in a quantum impurity model: Critical theory of the asymmetric pseudogap Kondo problem. *Phys. Rev. B* **70**, 094502 (2004).
60. Q. Si, G. Kotliar, Fermi-liquid and non-Fermi-liquid phases of an extended Hubbard model in infinite dimensions. *Phys. Rev. Lett.* **70**, 3143–3146 (1993).
61. Q. Si, G. Kotliar, Metallic non-Fermi-liquid phases of an extended Hubbard model in infinite dimensions. *Phys. Rev. B* **48**, 13881–13903 (1993).
62. D. G. Joshi, C. Li, G. Tarnopolsky, A. Georges, S. Sachdev, Deconfined critical point in a doped random quantum Heisenberg magnet. arXiv:1912.08822 (18 December 2019).
63. A. V. Chubukov, D. L. Maslov, First-Matsubara-frequency rule in a Fermi liquid. I. Fermionic self-energy. *Phys. Rev. B* **86**, 155136 (2012).
64. H. J. Vidberg, J. W. Serene, Solving the Eliashberg equations by means of N-point Padé approximants. *J. Low Temp. Phys.* **29**, 179–192 (1977).
65. R. E. V. Profumo, C. Groth, L. Messio, O. Parcollet, X. Waintal, Quantum Monte Carlo for correlated out-of-equilibrium nanoelectronic devices. *Phys. Rev. B* **91**, 245154 (2015).
66. C. Bertrand, S. Florens, O. Parcollet, X. Waintal, Reconstructing nonequilibrium regimes of quantum many-body systems from the analytical structure of perturbative expansions. *Phys. Rev. X* **9**, 041008 (2019).
67. P. Cha, N. Wentzell, O. Parcollet, A. Georges, E.-A. Kim, Linear resistivity and Sachdev-Ye-Kitaev (SYK) spin liquid behavior in a quantum critical metal with spin-1/2 fermions. Figshare. https://doi.org/10.6084/m9.figshare.12627419. Deposited 8 July 2020.